Monthly Notices of the ROYAL ASTRONOMICAL SOCIETY

MNRAS **532,** 2098–2107 (2024) https://doi.org/10.1093/mnras/stae1578
Advance Access publication 2024 June 25

Cosmic-ray confinement in radio bubbles by micromirrors

Robert J. Ewart [1,2★] Patrick Reichherzer,[1,3] Archie F. A. Bott,[1,4] Matthew W. Kunz[5,6] and Alexander A. Schekochihin[1,7]

[1]*Department of Physics, University of Oxford, Oxford, OX1 3PU, UK*
[2]*Balliol College, Oxford, OX1 3BJ, UK*
[3]*Exeter College, Oxford, OX1 3DP, UK*
[4]*Trinity College, Oxford, OX1 3BH, UK*
[5]*Department of Astrophysical Sciences, Princeton University, Peyton Hall, Princeton NJ 08544, USA*
[6]*Princeton Plasma Physics Laboratory, Princeton University, PO Box 451, Princeton NJ 08543, USA*
[7]*Merton College, Oxford OX1 4JD, UK*

Accepted 2024 June 20. Received 2024 June 4; in original form 2024 April 7

ABSTRACT

Radio bubbles, ubiquitous features of the intracluster medium around active galactic nuclei, are known to rise buoyantly for multiple scale heights through the intracluster medium (ICM). It is an open question how the bubbles can retain their high-energy cosmic-ray content over such distances. We propose that the enhanced scattering of cosmic rays due to micromirrors generated in the ICM is a viable mechanism for confining the cosmic rays within bubbles and can qualitatively reproduce their morphology. We discuss the observational implications of such a model of cosmic-ray confinement.

Key words: convection – diffusion – cosmic rays – galaxies: clusters: intracluster medium.

1 INTRODUCTION

Amongst the various morphologies exhibited in radio emission by active galaxies, one of the most prominent is the so-called radio 'bubble' (Fanaroff & Riley 1974; Churazov et al. 2000; Churazov et al. 2001; De Gasperin et al. 2012; Velović et al. 2023), christened as such by Gull & Northover (1973) for their analogy to bubbles of air rising through liquid. The brightness of these structures in radio (between several tens of MHz and a few GHz, Dunn, Fabian & Taylor 2005) being roughly consistent with an absence of X-rays (see e.g. Böhringer et al. 1993; Bîrzan et al. 2004; McNamara & Nulsen 2007) indicates that they are filled with high-energy particles emitting synchrotron radiation in the presence of a magnetic field. These bubbles are observed at a range of distances from the centres of cool-core clusters, where they are sourced by active galactic nuclei (AGN), implying there must be some mechanism, presumably magnetic in nature, by which high-energy cosmic rays (CRs) are confined to within the bubble for the duration of the bubble's rise. Recently, Reichherzer et al. (2023) have proposed that, within the ICM, the predominant scattering of sub-TeV CRs is due to deflections by small-scale 'micromirrors', which should arise naturally, generated by the mirror instability, in high-β plasmas such as the ICM (Schekochihin et al. 2005; Kunz, Jones & Zhuravleva 2022). In this paper, we show that such scattering is capable of efficiently confining CRs within bubbles, qualitatively mimicking the sharp boundary seen in radio emission.

The life of a typical bubble begins with the inflation of a radio lobe by the jet of an AGN. After initial supersonic expansion, the lobe is further slowly inflated in pressure balance with the ICM into which it is injected. By virtue of its underdensity with respect to the surrounding matter, the lobe begins to rise, eventually detaching from the AGN and becoming a bubble. Throughout the bubble's rise, it is deformed under the influence of hydrodynamic and magnetohydrodynamic effects (Churazov et al. 2001; Bruggen 2003). Such evolution has been studied extensively not only for its own sake, but also because the bubbles are considered to be a potent source of energy that can account for a significant portion of the heating required to obviate the cooling-flow problem and regulate AGN feedback (see e.g. Churazov et al. 2000; Peterson & Fabian 2006; McNamara & Nulsen 2007; Werner et al. 2018). The exact method by which this energy is deposited into the ICM has been the subject of numerous studies, both analytical and numerical (Churazov et al. 2001; Reynolds, Balbus & Schekochihin 2015; Bambic & Reynolds 2019; Chen, Heinz & Enßlin 2019).

Despite extensive studies of the various mechanisms by which the bubble deposits energy into the ICM, there is still some debate as to which mechanisms protect the bubbles from a host of hydrodynamic instabilities (see e.g. Ruszkowski et al. 2008; Guo et al. 2012; Kingsland et al. 2019). Putting aside the question of the longevity of the bubbles themselves, the sharp boundary of the bubble in radio and the lack of observed γ-ray emission in galaxy clusters (see e.g. Ahnen et al. 2016; Prokhorov & Churazov 2017) suggests that CRs are well confined within the bubble for long times until they eventually slowly leak out (e.g. De Gasperin et al. 2012). How they manage that is a question that remains open. Previous models for

★ E-mail: robert.ewart@balliol.ox.ac.uk

CR confinement in bubbles have relied on the large-scale magnetic-field structure around the bubble, viz., draping of magnetic fields over the bubble (see e.g. Dursi & Pfrommer 2008; Ruszkowski et al. 2008), or on the internal structure of the magnetic field, which are thought to confine CRs by exploiting the lack of field lines crossing the bubble boundary. However, such models may be vulnerable to the objection that any field lines that do connect the bubble's interior to its exterior, e.g., those that could be created by reconnection on the bubble's surface, would become a highway along which the CRs could escape (see e.g. Enßlin 2003).[1] Even in the absence of such violent escape of CRs, streaming along magnetic-field lines would naturally lead to significant variation in the extent of radio emission as a function of observed frequency – simply put, older CRs would have travelled further along magnetic-field structures creating extended emission at lower frequencies. This is precisely what is not seen in observations of radio bubbles (see e.g. De Gasperin et al. 2012; Brienza et al. 2021). We therefore propose that it is CR scattering off small-scale fluctuations in the weak magnetic field outside the bubble that, paradoxically, can serve as a good mechanism of confinement.

Intuitively the explanation for this form of confinement is as follows. CRs leaving the bubble in the direction of the bubble's motion find themselves scattering off fluctuations in the magnetic field, and becoming diffusive after a single mean free path. Like a ballistic tortoise racing against a diffusive hare, the bubble will continue its buoyant motion at roughly constant velocity, which overtakes the diffusive motion of the recently escaped CRs over sufficiently long times. This allows the bubble effectively to recapture some of the escaping CRs, maintaining the sharp boundary seen in observations (see e.g. De Gasperin et al. 2012; Brienza et al. 2021). In the rest frame of the bubble, this amounts to the CRs scattering in the flow sweeping past the bubble and thus being driven back onto the bubble. Underneath the bubble (i.e. in the opposite direction to the bubble velocity), the same diffusive behaviour applies, but CRs clearly cannot be swept back up. However, provided the bubble creates a sufficiently extended wake behind it (as indeed seen in numerical simulations, e.g. by Zhang, Churazov & Schekochihin 2018; Zhang et al. 2022), the flow immediately behind the bubble will also be rising, rendering the loss of CRs behind the bubble entirely diffusive.

Clearly, any diffusive process is necessarily a leaky and imperfect confinement mechanism. It must be the case that the CRs with larger diffusion coefficients escape from the bubble more easily. This can be quantified by the following, largely dimensional, argument (Mathews & Brighenti 2007). A CR escaping the bubble with a diffusion coefficient κ will, on average, travel a distance $\sim\sqrt{\kappa t}$ in time t. Even if the CR diffuses entirely vertically, the bubble, moving at speed u_b, will overtake the CR after a time $t \sim \kappa/u_\mathrm{b}^2$. Therefore, for the CR to escape the bubble rather than be recaptured, it must diffuse out of the path of the bubble – a horizontal distance comparable to the radius r_b of the bubble – in a time $t \sim \kappa/u_\mathrm{b}^2$. Hence, for CRs to be recaptured by the bubble upon their escape, their diffusivity must be sufficiently small so that

$$\frac{\kappa}{u_\mathrm{b} r_\mathrm{b}} \lesssim 1. \tag{1}$$

We will find that the conventionally estimated diffusivity of CRs, due to scattering by the streaming instability, is insufficient to satisfy equation (1) (Subedi et al. 2017; Krumholz et al. 2020). In contrast, the scattering mechanism proposed recently by Reichherzer et al. (2023) provides a sufficiently low diffusion coefficient to confine CRs below 1 TeV and reproduce the observed radio-bubble morphology.

The rest of this paper is structured as follows. In Section 2, we discuss the micromirror scattering mechanism for CRs below 1 TeV based on Reichherzer et al. (2023), and explain why the micromirrors should be endemic to the vicinity of the bubble. In Section 3, we show analytically and numerically that, even when the scattering centres are exclusively outside the bubble, the effect of the scattering can create a sharp bubble boundary with CRs confined either inside the bubble or within a thin layer of the ICM around it. Using the energy dependence of the scattering frequency, we obtain a prediction of how the thickness of this layer of CRs around the bubble should depend on particle energy. Furthermore, we show that the energy dependence of the scattering frequency gives rise to an interesting effusive behaviour, making the CR energy spectrum outside the bubble distinct from ('harder' than) that inside it. Finally, in Section 4, we summarize the progress that has been made and discuss the role of other sources of CR confinement.

2 DIFFUSIVITY DUE TO MICROMIRRORS

While typical estimates of the speed of bubble's buoyant rise through the ICM are on the order of the Keplerian velocity around the cluster centre (see e.g. Churazov et al. 2001), the CRs propagate at a velocity very close to the speed of light. In the absence of any forces therefore they would leave the bubble in a single light-crossing time. In reality, the bubble is permeated and surrounded by magnetic fields $\boldsymbol{B}$. These magnetic fields shape the velocity $\boldsymbol{v}$ of the CRs, forcing them to follow field lines in accordance with the Lorentz-force law, viz.,

$$\frac{\mathrm{d}\boldsymbol{v}}{\mathrm{d}t} = \frac{q}{m\gamma}\frac{\boldsymbol{v}\times\boldsymbol{B}}{c}, \tag{2}$$

where q and m are the charge and rest mass of the CR, respectively, and $\gamma = (1-|\boldsymbol{v}|^2/c^2)^{-1/2}$ is its Lorentz factor.

The confinement of field-line-following CRs can only be efficient if no field lines cross the bubble boundary. However, one might expect that reconnection on the bubble surface would quickly engender such stray field lines, reducing the effectiveness of confinement (see e.g. Enßlin 2003). In such cases, there must be some further effect limiting the escape of CRs along field lines. For example, a CR following the large-scale magnetic field will pitch-angle scatter off any small-scale (meaning smaller than the CR's gyroradius) fluctuating magnetic fields $\delta\boldsymbol{B}$, and thus migrate onto a different field line. After many such scatterings, its direction can entirely reverse. Following Reichherzer et al. (2023), we can use equation (2) to estimate the amount by which such a CR will be scattered by fluctuations of amplitude $\delta\boldsymbol{B}$ in a time δt[2]:

$$\frac{|\delta\boldsymbol{v}|}{c} \sim \frac{q\delta B}{\gamma mc^2}c\delta t \sim \frac{c\delta t}{r_\mathrm{g}}\frac{\delta B}{B}, \tag{3}$$

where $r_\mathrm{g} = \gamma mc^2/qB$ is the CR gyroradius. The CR will spend a time $\delta t \sim l/c$ traversing a magnetic fluctuation of typical scale l.

[1] In addition, the extent to which the uniformity of the draped field line influences CR confinement within inflated jets was investigated by Desiati & Zweibel (2014), concluding non-uniformities significantly boost diffusion across field lines, in the context of the much closer, and younger, Fermi bubbles (Yang et al. 2012).

[2] This is similar in spirit to models of resonant scattering (see e.g. Jokipii 1966; Blandford & Eichler 1987), the crucial difference being that, here, the scattering is non-resonant – off of structures of size much smaller than the CR gyroradius.

If the ICM is assumed to be infested with such structures and the deflections from each structure add up like a random walk, then equation (3) can be used to estimate the scattering frequency – the rate at which the pitch angle of a CR is changed by an order-unity amount – as

$$\nu_{\rm mm} \sim \frac{|\delta \boldsymbol{v}|^2}{c^2 \delta t} \sim \frac{cl}{r_{\rm g}^2} \left(\frac{\delta B}{B}\right)^2 . \tag{4}$$

This formula makes several features obvious. First, the scattering frequency strongly increases with decreasing CR gyroradius (or, equivalently, the CR energy, since the two are linearly proportional to each other for relativistic CRs). Secondly, and intuitively, the larger the relative amplitude of the fluctuating magnetic field, the more efficient will be the scattering of CRs. As pointed out by Reichherzer et al. (2023), in the ICM plasma, there are a myriad of ways of creating microscale magnetic fluctuations by kinetic instabilities enabled in the high-β regime (Schekochihin & Cowley 2006; Bott, Cowley & Schekochihin 2024). These kinetic instabilities arise because, in the high-β regime, low-Mach number turbulent motions are able to cause changes in the magnitude of the magnetic field, which in turn drive pressure anisotropies that compete with magnetic forces, and can excite ion-Larmor-scale kinetic instabilities. Amongst this family of instabilities, the mirror instability, generated in regions of increasing magnetic-field strength, is special in that it saturates with $\delta B/B \sim 1/3$ (Kunz, Schekochihin & Stone 2014; Riquelme, Quataert & Verscharen 2015; Melville, Schekochihin & Kunz 2016), making it a prime candidate for scattering CRs. Making a rough estimate of the relevant ICM parameters – that $l \sim 100$ npc (Rincon, Schekochihin & Cowley 2015) and $B \sim 3\,\mu$G (Kunz et al. 2022) – one finds the CR diffusion coefficient due to micromirrors to be (Reichherzer et al. 2023)

$$\kappa \sim 10^{30} \left(\frac{E}{\rm TeV}\right)^2 {\rm cm^2 s^{-1}}, \tag{5}$$

where E is the CR energy. Here, the key step is to compare it to the dimensional estimate (1). Noting the typical values of the bubble radius $r_{\rm b} \sim 5$–10 kpc and velocity $u_{\rm b} \sim 100$–$400\,{\rm km\,s^{-1}}$ (e.g. Zhang et al. 2018), one finds that

$$\frac{\kappa}{u_{\rm b} r_{\rm b}} \sim \left(\frac{E}{\rm TeV}\right)^2 \left(\frac{u_{\rm b}}{200\,{\rm km\,s^{-1}}}\right)^{-1} \left(\frac{r_{\rm b}}{10\,{\rm kpc}}\right)^{-1} . \tag{6}$$

This implies that, for energies much larger than a TeV, the diffusion coefficient is most likely too large to be of much assistance with CR confinement in bubbles. In contrast, for CR energies lower than a few 100 GeV, micromirror diffusion could indeed be consequential. While the precise value of the diffusion coefficient is subject to a number of factors (we refer the reader to Reichherzer et al. 2023 for details), it should be noted that the region of compressing (draped) magnetic field around the bubble, of characteristic size $\sim r_{\rm b}$ (see e.g. Dursi & Pfrommer 2008), creates the perfect environment for micromirrors to thrive because, as discussed above, mirrors are driven by positive pressure anisotropy, which is created in regions where the magnetic field's strength is increasing.

One could still object that it is unclear how small one requires the ratio in equation (6) to be for good confinement, or indeed whether some power of the dimensionless factor of $c/u_{\rm b}$ should appear for some unknown reason. We must therefore scope out whether our picture of the bubbles can hold water, or indeed CRs. This is done, both numerically and analytically, in the next section.

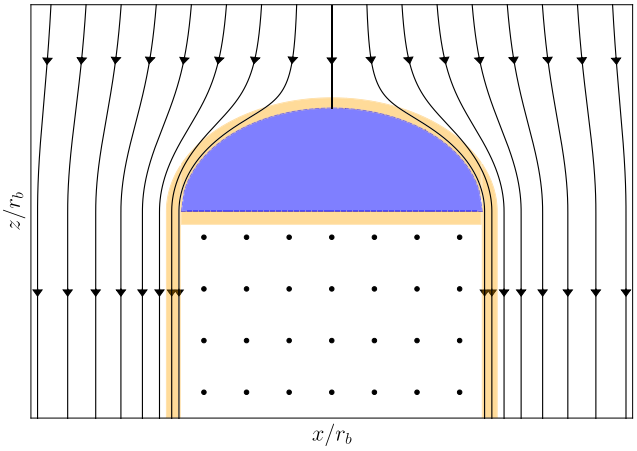

Figure 1. A schematic of a 2D slice of the fluid flow around the bubble used for our mock simulation. The blue-shaded region represents the nominal interior of the bubble, in which the CRs propagate ballistically. The expected area in which CRs will diffuse off the bubble is shaded in orange. The arrowed black lines are the streamlines of the flow around the bubble. Beneath the bubble, the flow is stationary in the rest frame of the bubble, crudely approximating a wake.

3 PROOF OF CONCEPT AND MOCK SIMULATION

We first investigate our model of confinement numerically. Clearly, a full solution to the problem would require an accurate magnetohydrodynamic model of the nearly collisionless ICM coupled to a kinetic or fluid model of CRs (see e.g. Zweibel 2017; Weber, Thomas & Pfrommer 2022). However, the choice of a fluid magnetohydrodynamic model in a nearly collisionless environment is still an open area of research (see e.g. Squire et al. 2019; Kunz et al. 2022; Squire et al. 2023; Majeski, Kunz & Squire 2024), as is the fluid dynamics of CRs. Furthermore, many studies of the buoyant rise of bubbles are plagued by hydrodynamic instabilities that shred the bubbles long before they have risen to the distances at which they are observed (e.g. Dong & Stone 2009; Reynolds et al. 2015). We therefore take an extremely simplified toy model in which the flow is externally prescribed. Such an approach may be partially justified a posteriori, should we find that the CRs are well confined within the bubble (which we will), since there is then at least no inconsistency with the bubble having a boundary.

The details of the numerical simulation are presented in Appendix A. The basic concept of it is as follows. Within the bubble, the CRs move ballistically as if under no force. This is clearly a simplification of the exact, field-line following trajectory that the CRs will take. Outside the bubble, the CRs scatter off micromirrors, but crucially, they do so in the rest frame of the flow $\boldsymbol{u}$ that they encounter, because mirror-unstable fluctuations have no phase velocity relative to the bulk plasma. We take the imposed flow to be a 3D, incompressible, irrotational flow above a half-sphere, while below the sphere, to simulate the effect of a wake, the flow is taken to be entirely vertical. A schematic of this flow is shown in Fig. 1, the explicit expressions for it are given in Appendix A. Clearly, the wake of this bubble is a major simplification, since it effectively implies that the bubble causes a rigid column of fluid to rise behind it. Simulations with rigid bubbles have exhibited wakes that extend over several tens of kiloparsecs entraining a large amount of material, albeit via vortices, in the wake of the bubble (e.g. Zhang et al.

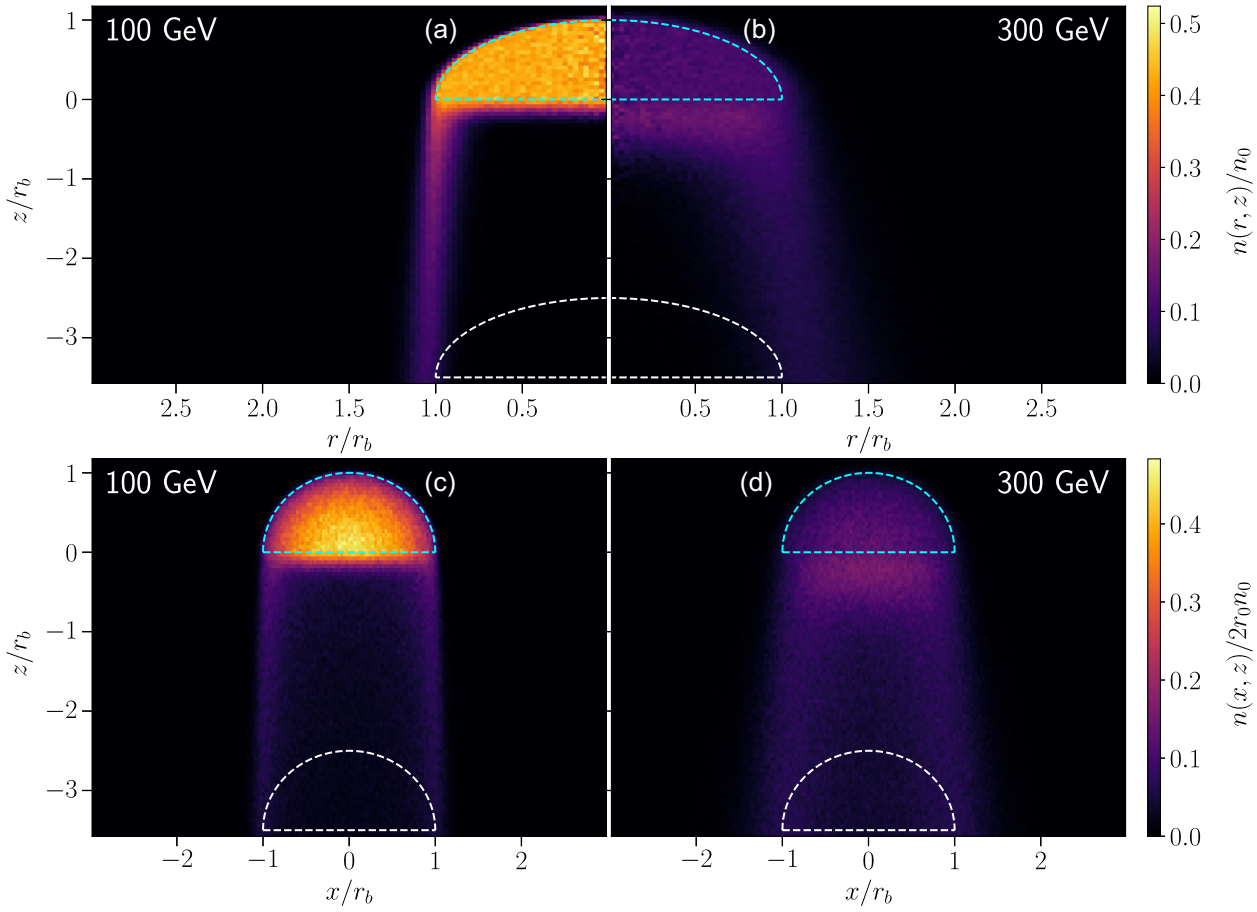

Figure 2. The density of CRs was attained numerically with populations at distinct energies (100 and 300 GeV), and therefore diffusion coefficients, after the bubble rose a distance of $3.5r_b$. Both bubbles were chosen to have a radius of 10 kpc and to rise at constant velocity of 200 km s^{-1}. Panels (a) and (b) show the azimuthally averaged densities, panels (c) and (d) show the same densities in projection. The densities are normalized to the maximum value that the initial density (all CRs inside the bubble) could take in that projection. Dashed lines indicate the initial (white) and final (blue) positions of the nominal boundary of the bubble.

2022). We therefore do not hope to capture accurately the density of CRs within the wake. Rather, we include the rising column to ensure that there is no spurious flow beneath the bubble capable of stealing CRs directly from it. This toy model will prove sufficient to illustrate the physics relevant to our proposed theory of CR confinement.

Our central result – that scattering by micromirrors efficiently confines CRs of low energy – is illustrated in Fig. 2, which shows the density (normalized to the initial density $n_0 = 3N/2\pi r_b^3$ of N CRs in a hemisphere of radius r_b) of two populations of CRs initialized at two different energies after the bubble has risen to a height equal to 3.5 times its radius, which was taken to be 10 kpc for these simulations. The CRs at 100 GeV are confined remarkably well to the bubble, while the CRs at 300 GeV have leaked out of the bubble left, right, centre, and, predominantly, downwards. As anticipated, we see that the upstream bubble boundary is much thinner than the bubble for both energies because the CRs are being swept back onto the bubble.

In what concerns the situation beneath the bubble, Fig. 2 provides an immediate refinement to our picture of how bubbles leak CRs. All leakage occurs via the sides of the bubble as the CRs that diffuse horizontally are swept away with the flow (see the shaded orange region of Fig. 1). Clearly, for lower-energy CRs, one can estimate the rate of loss from the volume of ICM containing CRs that is swept away from bubble. This statement can be made more quantitative in the following way: Around the bubble, there is a thin layer, of width Δr, containing CRs embedded in the ICM flow. In a short time Δt, the bubble sheds a cylindrical shell of height $\sim u_b \Delta t$ of this layer due to the flow dragging it away. If the CR density in the bubble and layer is roughly n, then the number of CRs lost in this short time is of order $2\pi r_b n u_b \Delta t \Delta r$. Since the lost CRs come from the bubble, this gives us an estimate for the time dependence of the bubble density:

$$\frac{2\pi}{3} r_b^3 \frac{\mathrm{d}n}{\mathrm{d}t} \sim -2\pi r_b n u_b \Delta r \Rightarrow \frac{\mathrm{d}n}{\mathrm{d}t} \sim -3\frac{u_b \Delta r}{r_b^2} n. \tag{7}$$

Thus, we see that the rate of the CR loss depends crucially on the width Δr of the layer of CRs draped over the bubble. To determine this width, we turn towards a toy analytical model for the diffusion of CRs around the bubble.

3.1 The Blasius boundary layer and CR confinement time

As discussed above, the correct model for the hydrodynamics of CRs is an open area of research. However, for our toy model, we again take the simplest possible approximation for the evolution of the CR density outside the bubble. The CRs of any given energy

diffuse with a diffusion coefficient κ and are advected by the velocity field $\boldsymbol{u}$. Thus, outside the bubble, a model equation for the CR density n is

$$\frac{\partial n}{\partial t} + \boldsymbol{u} \cdot \nabla n = \kappa \nabla^2 n. \tag{8}$$

Of course, this equation neglects a number of things.

First, it neglects any changes in the CR energy, and hence the resulting changes in their diffusion coefficient, due to acceleration mechanisms left outside our model (such as synchrotron losses), or indeed due to Fermi (1949) acceleration from scattering in the rest frame of the flow, which is present in our model. While neglecting these losses may be appropriate for CR ions, we may justify the neglect of synchrotron losses for CR leptons by noting that the typical synchrotron loss time is $t_{\rm sync} \sim 10^7 (B/\mu{\rm G})^{-2} (E/{\rm TeV})^{-1}$ yr (see e.g. Jackson 1998; HESS Collaboration et al. 2016). While this could be comparable to the bubble rise time for energies near a TeV, it is likely to be a subdominant effect for energies closer to a few GeV. As for Fermi acceleration, since the flow speed is a small fraction of the speed of light, we can expect the acceleration to be relatively weak over the time-scales that we are considering (we justify this *a posteriori* in Appendix B).

Secondly, the CR density within the bubble itself is not specified by equation (8). Thankfully, the light-crossing time $r_{\rm b}/c$, which is the time-scale on which density perturbations will be ironed out inside the bubble, is much shorter than the bubble rise time $r_{\rm b}/u_{\rm b}$. As a result, the CR density in the bubble interior only functions as a boundary condition fixing the density at the bubble-ICM interface. This boundary condition will evolve in time as the density within the bubble decreases, but, provided the confinement is good, this boundary condition will evolve slowly allowing the density of CRs outside the bubble to reach a quasi-steady profile with an amplitude set by their density at the boundary.

The solution of the advection–diffusion equation (8) near a boundary is a well-studied topic (see e.g. Batchelor 1967; Landau & Lifshitz 1987). In the ICM above the bubble, this problem is mathematically identical to the problem of the width of cold fronts due to thermal conduction (studied, for instance, by Churazov & Inogamov 2004; Xiang et al. 2007) with CR density taking the place of temperature. According to Xiang et al. (2007), a boundary layer of thickness Δr given by

$$\frac{\Delta r}{r_{\rm b}} \sim \sqrt{\frac{\kappa}{u_{\rm b} r_{\rm b}}} \tag{9}$$

forms around the surface of the bubble. This is obvious if one notes that, in a steady state, the diffusive term in equation (8) pushing CRs away from the bubble must balance the advective term sweeping them back onto the bubble; since the diffusive term scales as $\kappa n/\Delta r^2$ and the advective term scales as $u_{\rm b} n/r_{\rm b}$, one immediately arrives at equation (9). The full solution and scaling analysis of equation (8), extended to the entire region $0 \leq \theta \leq \pi/2$, are given in Appendix C. Combining the estimate (9) for the width of the layer with equation (6) for the CR diffusion coefficient upgrades the estimate (7) of the density depletion rate to (neglecting constants of order unity)

$$\frac{1}{n}\frac{{\rm d}n}{{\rm d}t} \sim -\frac{u_{\rm b}}{r_{\rm b}} \sqrt{\frac{\kappa(E)}{u_{\rm b} r_{\rm b}}}, \tag{10}$$

giving a typical confinement time

$$t_{\rm conf} \sim \left(\frac{E}{\rm TeV}\right)^{-1} \left(\frac{u_{\rm b}}{200\,{\rm km\,s^{-1}}}\right)^{-1/2} \left(\frac{r_{\rm b}}{10\,{\rm kpc}}\right)^{3/2} 100\,{\rm Myr}. \tag{11}$$

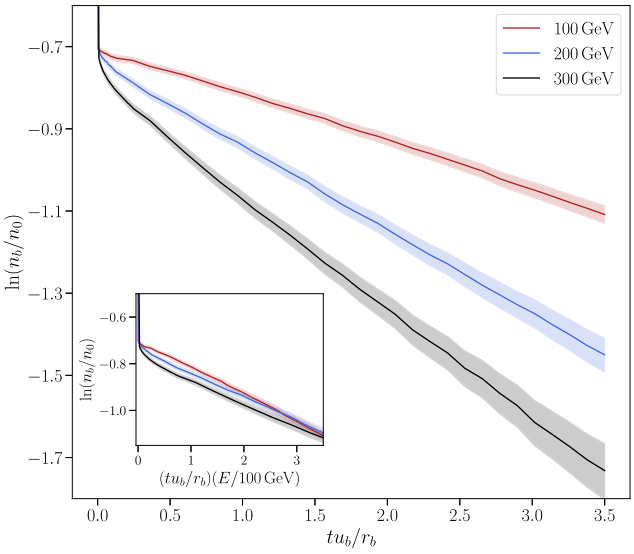

Figure 3. The time evolution of the CR density within bubbles (with shading showing error bars of two standard deviations) initialized with CRs at three different energies, 100, 200, 300 GeV. Inset shows the same evolution with the time axis scaled by the initial CR energy, which is the relevant variable in our order-of-magnitude estimate (10).

A comparison with the results of numerical simulation in Fig. 3 shows good agreement with the general trend[3]

This result shows that the use of the micromirror model of Reichherzer et al. (2023) is essential. As discussed in Reichherzer et al. (2023), CR diffusion due to the more conventional scattering mechanisms (turbulence, streaming instability, etc.) is comparable to the diffusion due to micromirrors for ∼1 TeV CRs. From equation (10) and Fig. 3, we see therefore that those conventional scattering schemes would be incapable of confining CRs efficiently.

3.2 Hardening of CR spectrum outside bubbles

The equation (10) has an energy dependence, which provides an observationally intriguing possibility for the radio bubbles. Since the CRs of higher energies escape the bubble faster, this bears a certain resemblance to an effusive process: CRs with higher energies will be overrepresented outside the bubble – a feature which is general to many CR systems with energy-dependent escape times (see e.g. Matthews & Taylor 2021).

To make this statement more quantitative, consider the following argument. From equation (10), we may assume that the distribution of particle energies within the bubble will have form

$$f(E) = f_0(E) \exp\left[-\alpha \sqrt{\frac{\kappa(E)}{u_{\rm b} r_{\rm b}}} \frac{u_{\rm b} t}{r_{\rm b}}\right], \tag{12}$$

where α is some order-unity constant related to the precise nature of the flow. The energy dependence enters via the injected spectrum $f_0(E)$ and the diffusion coefficient $\kappa(E)$. For times earlier than the characteristic loss time in equation (11) of CRs at a given energy, the

[3]We note that the CR confinement time is longer than the typical (leptonic) synchrotron loss time $\sim 10^7 (B/\mu{\rm G})^{-2} (E/{\rm TeV})^{-1}$ yr, which itself is longer than the typical bubble rise time. This should imply that the CR leptons will gradually age as the bubble rises, slowly reducing their average diffusion coefficient and potentially lengthening their confinement time further.

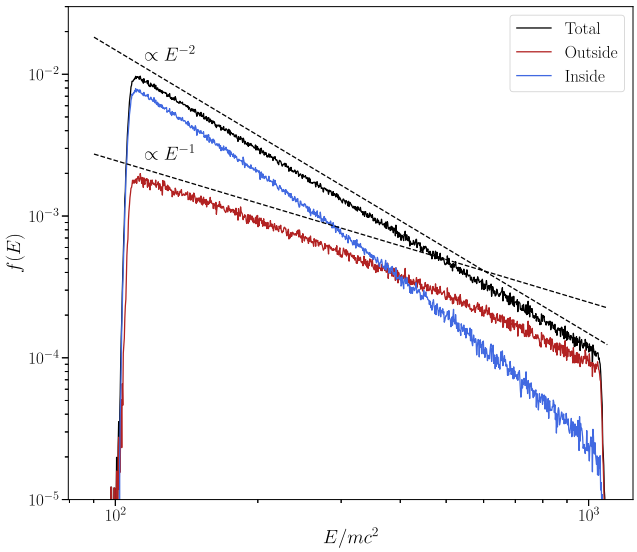

Figure 4. The distribution function $f(E)$ of CR energies inside (blue) and outside (red) of the bubble after the bubble has risen $0.5r_b$. The total distribution of all CRs is shown in black. For this simulation, CRs were sourced inside the bubble with a distribution of energies $\propto E^{-2}$. CRs of higher energies preferentially leak from the bubble, hardening the spectra outside the bubble in agreement with equation (13).

exponent in equation (12) will be small. While the CR distribution inside the bubble will therefore change little, outside the bubble the distribution will be

$$f_{\rm out}(E) = f_0(E)\left\{1-\exp\left[-\alpha\sqrt{\frac{\kappa(E)}{u_b r_b}}\frac{u_b t}{r_b}\right]\right\}$$
$$\sim f_0(E)\alpha\sqrt{\frac{\kappa(E)}{u_b r_b}}\frac{u_b t}{r_b} \propto f_0(E)E, \qquad (13)$$

the last proportionality following from equation (6). Thus, the CR spectrum will be hardened by a factor of E outside the bubble. We confirm this result in Fig. 4, which indeed shows the hardening of the CR spectra of CRs outside the bubble. This also offers an explanation for the hardening of the CR spectrum outside radio filaments recently reported in the giant fossil radio lobe of the Ophiuchus galaxy cluster (Giacintucci, Markevitch & Clarke 2024).

Another way of understanding this effect is as follows. The typical density of the layer of CRs around the bubble will be $\propto f_0(E)$ since the density of CRs must be continuous across the boundary. However, the boundary-layer width Δr is a function of energy in equation (9), $\Delta r \propto E$, so the distribution of energies outside the bubble and in the wake will be proportional to the density imposed by the source multiplied by this width.

4 CONCLUSION AND DISCUSSION

We have proposed a new model for the confinement of CRs within radio bubbles, offering a possible explanation for the sharp boundaries seen in radio observation of these bubbles. While the model is simple in nature, being based straightforwardly on the competition between advection and diffusion of CRs, its success hinges on the enhanced CR scattering proposed by Reichherzer et al. (2023). We confirm numerically (see Fig. 2) that such an enhanced scattering does indeed provide good confinement of sub-TeV CRs and argue that the alternative, more conventional schemes for CR scattering at such energies are too weak to provide adequate CR confinement via isotropic diffusion. Finally, we note that the energy dependence of the CR diffusion coefficient has an interesting observational implication for the observed CR spectrum outside the bubble, which we predict (provided it has not been significantly aged by radiation losses) to be one power of energy shallower than the source spectrum (see Fig. 4), due to the greater ease with which high-energy CRs can leave the bubble.

A promising consequence of the long, energy-dependent confinement time in equation (11) of CRs is that it is on the same order as, and not in great excess of, the lower bound on confinement time inferred by Prokhorov & Churazov (2017) from the lack of observed gamma-ray emission. While the two estimates should not be directly compared like for like (as their model assumed energy-independent escape and diffusion time-scales), the proximity of the two estimates implies that diffusion of CRs in micromirrors could play an important role in constraining the energetic content of the bubbles (see e.g. Yang, Gaspari & Marlow 2019; Beckmann et al. 2022; Ruszkowski & Pfrommer 2023).

A number of approximations have been made in order to arrive at these conclusions. One of our more extreme modelling assumptions is the artificial imposition of the bubble boundary and flow profile. While we anticipate that the true velocity field around the bubble will be different in detail from that assumed by us, it will undoubtedly contain a wake and a flow around the bubble, which are the only essential ingredients in our picture. This does, however, presuppose the integrity of the bubble to hydrodynamic instabilities, which would otherwise shred it. While the enhanced scattering offered by micromirrors can adequately confine CRs, those same micromirrors may also suppress the ICM viscosity (see e.g. Kunz et al. 2014; Melville et al. 2016). Should the ICM viscosity be overly suppressed, this would lead to a disruption of bubbles, which we clearly do not see (see discussion in, e.g., Ruszkowski et al. 2008; Kingsland et al. 2019). Of course, for our model to work, it is sufficient to have only the immediate vicinity of the bubble's boundary infested by micromirrors, since the CRs do not sample a large volume around the bubble. As discussed in Section 2, one could therefore envision a possibility where micromirrors are localized to the area of increasing magnetic-field strength around the bubble (where they are naturally driven unstable by the resulting pressure anisotropy), while the ICM at large may have a much smaller fraction of its volume filled by micromirrors. Furthermore, the same pressure anisotropy that creates the micromirrors also enhances the effective tension force exerted by the magnetic draping, potentially protecting the bubble from hydrodynamic instabilities in spite of the lower viscosity.

We also do not capture the effects of bubble deformation (Guo 2015) and the back reaction of the CRs on the bubble. Should such back reaction be included, it is now clear that it must also include the enhanced diffusion of CRs by micromirrors, if for no other reason than that the dimensional estimate (6) ensures its *a priori* non-negligibility. As for the effects of bubble growth and of the variation in the flow speed, our model suggests the advantageous picture that the bubble will actually become *better* at confining CRs as it rises, because one expects the bubbles to slow down and grow, increasing the confinement time in equation (11), $t_{\rm conf} \propto u_b^{-1/2} r_b^{3/2}$. This perhaps points to the possibility that CR scattering, especially by micromirrors, as a confinement mechanism could be effective for a wide range of ICM radio features that account for the earlier or later stages of the bubble's life, such as filamentary structures, lobes, or jets.

ACKNOWLEDGEMENTS

It is a pleasure to thank Georgia Acton, Eugene Churazov, Plamen Ivanov, Philipp Kempski, Hrushikesh Loya, Michael Nastac, Marcel Rod, Luis Silva, and Dmitri Uzdensky for illuminating discussions. The work was also improved by the recommendation of an anonymous reviewer RJE was supported by a UK EPSRC studentship, PR by a Gateway Fellowship and Walter-Benjamin Fellowship, AFAB by a UKRI Future Leaders Fellowship (grant number MR/W006723/1), MWK in part by NSF CAREER Award No. 1944972; the work of AAS was supported in part by grants from STFC (ST/W000903/1) and EPSRC (EP/R034737/1), as well as by the Simons Foundations via a Simons Investigator award.

DATA AVAILABILITY

The data underlying this article will be shared on reasonable request to the corresponding author.

REFERENCES

Ahnen M. L. et al., 2016, A&A, 589, A33
Bambic C. J., Reynolds C. S., 2019, ApJ, 886, 78
Batchelor G., 1967, An Introduction to Fluid Dynamics. Cambridge Univ. Press, Cambridge
Beckmann R. S., Dubois Y., Pellissier A., Olivares V., Polles F. L., Hahn O., Guillard P., Lehnert M. D., 2022, A&A, 665, A129
Bîrzan L., Rafferty D. A., McNamara B. R., Wise M. W., Nulsen P. E. J., 2004, ApJ, 607, 800
Blandford R., Eichler D., 1987, Phys. Rep., 154, 1
Böhringer H., Voges W., Fabian A. C., Edge A. C., Neumann D. M., 1993, MNRAS, 264, L25
Bott A. F., Cowley S., Schekochihin A., 2024, J. Plasma Phys, 90, 975900207
Brienza M. et al., 2021, Nat. Astron., 5, 1261
Bruggen M., 2003, ApJ, 592, 839
Chen Y.-H., Heinz S., Enßlin T. A., 2019, MNRAS, 489, 1939
Churazov E., Inogamov N., 2004, MNRAS, 350, L52
Churazov E., Forman W., Jones C., Böhringer H., 2000, A&A, 356, 788
Churazov E., Bruggen M., Kaiser C. R., Bohringer H., Forman W., 2001, ApJ, 554, 261
De Gasperin F. et al., 2012, A&A, 547, A56
Desiati P., Zweibel E. G., 2014, ApJ, 791, 51
Dong R., Stone J. M., 2009, ApJ, 704, 1309
Dunn R. J. H., Fabian A. C., Taylor G. B., 2005, MNRAS, 364, 1343
Dursi L., Pfrommer C., 2008, ApJ, 677, 993
Enßlin T. A., 2003, A&A, 399, 409
Fanaroff B. L., Riley J. M., 1974, MNRAS, 167, 31P
Fermi E., 1949, Phys. Rev., 75, 1169
Giacintucci S., Markevitch M., Clarke T. E., 2024, RMxAC, 56, 48
Gull S. F., Northover K. J. E., 1973, Nature, 244, 80
Guo F., 2015, ApJ, 803, 48
Guo F., Mathews W. G., Dobler G., Oh S. P., 2012, ApJ, 756, 182
HESS Collaboration et al., 2016, Nature, 531, 476
Jackson J., 1998, Classical Electrodynamics. Wiley, Hoboken
Jokipii J. R., 1966, APJ, 146, 480
Kingsland M., Yang H.-Y. K., Reynolds C. S., Zuhone J. A., 2019, ApJ, 883, L23
Krumholz M. R., Crocker R. M., Xu S., Lazarian A., Rosevear M. T., Bedwell-Wilson J., 2020, MNRAS, 493, 2817
Kunz M. W., Schekochihin A. A., Stone J. M., 2014, Phys. Rev. Lett., 112, 205003
Kunz M. W., Jones T. W., Zhuravleva I., 2022, in Handbook of X-ray and Gamma-ray Astrophysics. Springer Nature, Singapore
Landau L., Lifshitz E., 1987, Fluid Mechanics: Volume 6. Pergamon, New York
Lemoine M., 2019, Phys. Rev. D, 99, 083006
Majeski S., Kunz M. W., Squire J., 2024, preprint (arXiv:2405.02418)
Mathews W. G., Brighenti F., 2007, ApJ, 660, 1137
Matthews J. H., Taylor A. M., 2021, MNRAS, 503, 5948
McNamara B., Nulsen P., 2007, Ann. Rev. Astron. Astrophys., 45, 117
Melville S., Schekochihin A. A., Kunz M. W., 2016, MNRAS, 459, 2701
Peterson J., Fabian A., 2006, Phys. Rep., 427, 1
Prokhorov D. A., Churazov E., 2017, MNRAS, 470, 3388
Reichherzer P., Bott A. F. A., Ewart R. J., Gregori G., Kempski P., Kunz M. W., Schekochihin A. A., 2023, preprint (arXiv:2311.01497)
Reynolds C. S., Balbus S. A., Schekochihin A. A., 2015, ApJ, 815, 41
Rincon F., Schekochihin A. A., Cowley S. C., 2015, MNRAS, 447, L45
Riquelme M. A., Quataert E., Verscharen D., 2015, ApJ, 800, 27
Ruszkowski M., Pfrommer C., 2023, Astron. Astrophys. Rev., 31, 4
Ruszkowski M., Enßlin T. A., Brüggen M., Begelman M. C., Churazov E., 2008, MNRAS, 383, 1359
Schekochihin A. A., Cowley S. C., 2006, Phys. Plasmas, 13, 056501
Schekochihin A. A., Cowley S. C., Kulsrud R., Hammett G., Sharma P., 2005, ApJ, 629, 139
Squire J., Schekochihin A. A., Quataert E., Kunz M. W., 2019, J. Plasma Phys., 85, 905850114
Squire J., Kunz M., Arzamasskiy L., Johnston Z., Quataert E., Schekochihin A., 2023, J. Plasma Phys., 89, 905890417
Subedi P. et al., 2017, ApJ, 837, 140
Velović V., Cotton W. D., Filipović M. D., Norris R. P., Barnes L. A., Condon J. J., 2023, MNRAS, 523, 1933
Weber M., Thomas T., Pfrommer C., 2022, MNRAS, 519, 3819
Werner N., McNamara B. R., Churazov E., Scannapieco E., 2018, Space Sci. Rev., 215, 5
Xiang F., Churazov E., Dolag K., Springel V., Vikhlinin A., 2007, MNRAS, 379, 1325
Yang H.-Y. K., Ruszkowski M., Ricker P. M., Zweibel E. G., Lee D., 2012, ApJ, 761, 185
Yang H.-Y. K., Gaspari M., Marlow C., 2019, ApJ, 871, 6
Zhang C., Churazov E., Schekochihin A. A., 2018, MNRAS, 478, 4785
Zhang C., Zhuravleva I., Gendron-Marsolais M.-L., Churazov E., Schekochihin A. A., Forman W. R., 2022, MNRAS, 517, 616
Zweibel E. G., 2017, Phys. Plasmas, 24, 055402

APPENDIX A: NUMERICAL DETAILS OF MOCK SIMULATION

In this appendix, we detail the numerical scheme by which the bubble and CRs were evolved in the mock numerical simulations whose results we presented in Figs 2–4. We use the Monte Carlo method, initializing a large number of CRs uniformly inside the boundary of the bubble. There are then two principal components in the simulation: the specification of the fluid flow in the rest frame of the bubble and the evolution equations for the CRs. We discuss the two separately, in turn.

A1 Fluid flow around the bubble

As illustrated in Fig. 1, the fluid flow that we impose is a 3D potential flow around a hemispherical cap representing the bubble, with an entrained wake represented by a column of fluid behind the bubble. It is known that the flow around a spherical object is well approximated by an incompressible, steady, irrotational flow (used as a reasonable approximation in the high-β plasma above the bubble, as in, e.g. Dursi & Pfrommer 2008). However, behind

the bubble, such a flow would not capture the turbulent wake that is formed. To model this turbulent wake in the most brutal fashion possible, we continue the streamlines vertically downward from the incompressible, steady, irrotational flow imposed above the sphere. This generates an incompressible rotational flow that describes the bubble dragging a column of fluid upwards from beneath it. The flow field in cylindrical coordinates z, r, φ will have azimuthal symmetry and be given by the vector field $\boldsymbol{u}(z, r) = u_z(z, r)\boldsymbol{e}_z + u_r(z, r)\boldsymbol{e}_r$, where the vertical velocity is

$$u_z(z,r) = \begin{cases} -v_\mathrm{b}\left[1 - r_\mathrm{b}^3 \frac{2z^2 - r^2}{2(z^2+r^2)^{5/2}}\right] & \text{for } z > 0, z^2 + r^2 > r_\mathrm{b}^2, \\ -v_\mathrm{b}\left(1 + \frac{r_\mathrm{b}^3}{2r^3}\right) & \text{for } z < 0, r > r_\mathrm{b}, \\ 0 & \text{otherwise,} \end{cases} \tag{A1}$$

and the radial velocity is

$$u_r(z,r) = \begin{cases} v_\mathrm{b} r_\mathrm{b}^3 \dfrac{3zr}{2(z^2+r^2)^{5/2}} & \text{for } \quad z > 0, z^2 + r^2 > r_\mathrm{b}^2, \\ 0 & \text{otherwise.} \end{cases} \tag{A2}$$

A2 Cosmic-ray evolution

To model CR propagation, we associate to each CR initially a position $\boldsymbol{x}$, an orientation $\boldsymbol{n}$, and a gamma factor γ. Then the question is how to step the position, orientation, and gamma factor forward in time. We know from equation (6) that the diffusion coefficient should be a function of the CR energy $E = \gamma mc^2$, and therefore of γ. As the simplest model of diffusive scattering possible, we consider the case where the CRs propagate for a time $1/\nu(\gamma)$, whereupon, if they find themselves outside the bubble, they are isotropically scattered in the rest frame of the flow. Explicitly this means that if $\boldsymbol{x}(t)$, $\boldsymbol{n}(t)$, and $\gamma(t)$ are the position, orientation, and gamma factor of a CR at time t, then its position at time $t + \Delta t$ is simply

$$\boldsymbol{x}(t + \Delta t) = \boldsymbol{x}(t) + c\Delta t \frac{\sqrt{\gamma(t)^2 - 1}}{\gamma(t)} \boldsymbol{n}(t), \tag{A3}$$

where $\Delta t = 1/\nu(\gamma(t))$. To find $\gamma(t)$ at the next time-step, we first compute its value $\tilde{\gamma}$ in the frame moving with the local flow $\boldsymbol{u}(\boldsymbol{x}(t + \Delta t))$:

$$\tilde{\gamma}(t) = \gamma_{\boldsymbol{u}}(\boldsymbol{x}(t + \Delta t)) \left[\gamma(t) - \sqrt{\gamma(t)^2 - 1} \frac{\boldsymbol{n}(t) \cdot \boldsymbol{u}(\boldsymbol{x}(t + \Delta t))}{c}\right], \tag{A4}$$

where $\gamma_{\boldsymbol{u}}$ is the gamma factor of the local flow, evaluated at $\boldsymbol{x}(t + \Delta t)$ – very close to unity, but included for completeness. The CR will scatter to a random orientation, denoted $\tilde{\boldsymbol{n}}$ – isotopic in the rest frame of the flow. Boosting back into the laboratory frame, we use the scattered orientation $\tilde{\boldsymbol{n}}$ to find the value of the gamma factor at the next time-step:

$$\gamma(t + \Delta t) = \gamma_{\boldsymbol{u}}(\boldsymbol{x}(t + \Delta t)) \left[\tilde{\gamma}(t) + \sqrt{\tilde{\gamma}(t)^2 - 1} \frac{\tilde{\boldsymbol{n}} \cdot \boldsymbol{u}(\boldsymbol{x}(t + \Delta t))}{c}\right], \tag{A5}$$

and the scattered orientation in the laboratory frame:

$$\begin{aligned} \boldsymbol{n}(t + \Delta t) = {} & \frac{\sqrt{\tilde{\gamma}(t)^2 - 1}}{\sqrt{\gamma(t + \Delta t)^2 - 1}} \Bigg\{ \tilde{\boldsymbol{n}} + \\ & + [\gamma_{\boldsymbol{u}}(\boldsymbol{x}(t + \Delta t)) - 1] \frac{\tilde{\boldsymbol{n}} \cdot \boldsymbol{u}(\boldsymbol{x}(t + \Delta t))}{|\boldsymbol{u}(\boldsymbol{x}(t + \Delta t))|} \frac{\boldsymbol{u}(\boldsymbol{x}(t + \Delta t))}{|\boldsymbol{u}(\boldsymbol{x}(t + \Delta t))|} \Bigg\} \\ & + \frac{\tilde{\gamma}(t)\gamma_{\boldsymbol{u}}}{\sqrt{\gamma(t + \Delta t)^2 - 1}} \frac{\boldsymbol{u}(\boldsymbol{x}(t + \Delta t))}{c}, \end{aligned} \tag{A6}$$

which naturally satisfies $|\boldsymbol{n}| = 1$ at each time-step.

APPENDIX B: ENERGIZATION OF COSMIC RAYS

While the numerical method presented in Appendix A allows for the variation in the energy of the CRs due to Fermi (1949) acceleration (i.e. energy gain via scattering off moving parcels of fluid), this process is ignored in our theoretical considerations of the boundary layer thickness and CR confinement time in Section 3. In this appendix, we justify this omission, showing that energization of CRs due to Fermi acceleration is at most an order-unity effect, and typically negligible.

Fig. B1(a) shows the energy distribution after the bubble has risen $3.5r_\mathrm{b}$ of a population of CRs initialized at 100 GeV. We see, by eye, that the change of energy is largely diffusive and that it is typically on the order of ∼5 per cent. That the energy change should be diffusive is expected for Fermi acceleration (see e.g. Lemoine 2019 and references therein). Furthermore, Fig. B1(b) tells us that the CRs that have diffused most in energy are found in the population escaped from the bubble. This is a simple matter to explain, as the CRs that have escaped from the bubble are likely to have undergone many scatterings on its surface, diffusing the furthest in energy.

To make this statement more quantitative, we note that the strongest kicks in Fermi acceleration should come from the CRs crossing from the bubble interior, where the flow is stationary (in the rest frame of the bubble), to the flow outside the bubble, with speed $\sim u_\mathrm{b}$, experiencing a relative change in energy $\sim u_\mathrm{b}/c$. The typical CR will make many such crossings of the bubble boundary, each time being recaptured, until it eventually escapes after a time t_conf given by equation (11). Since it takes a time $\sim r_\mathrm{b}/c$ to cross the bubble, the number of crossings of the bubble boundary that a typical CR will make before escaping is

$$N_\mathrm{esc} \sim \frac{c}{u_\mathrm{b}} \sqrt{\frac{u_\mathrm{b} r_\mathrm{b}}{\kappa}}. \tag{B1}$$

Since changes of the CR energy made in each crossing add up as a random walk, the typical energy change before escape will be

$$\begin{aligned} \frac{\Delta E}{E} &\sim \frac{u_\mathrm{b}}{c}\sqrt{N_\mathrm{esc}} \sim \sqrt{\frac{u_\mathrm{b}}{c}} \left(\frac{u_\mathrm{b} r_\mathrm{b}}{\kappa}\right)^{1/4} \\ &\sim 0.03 \left(\frac{E}{\mathrm{TeV}}\right)^{-1/2} \left(\frac{u_\mathrm{b}}{200\,\mathrm{km\,s^{-1}}}\right)^{3/4} \left(\frac{r_\mathrm{b}}{10\,\mathrm{kpc}}\right)^{1/4}. \end{aligned} \tag{B2}$$

This is in rough agreement with the ∼10–20 per cent acceleration/deceleration for 100 GeV CRs seen in Fig. B1. This tells us that we can expect order-unity energy changes for the lowest-energy CRs (those of a few GeV).

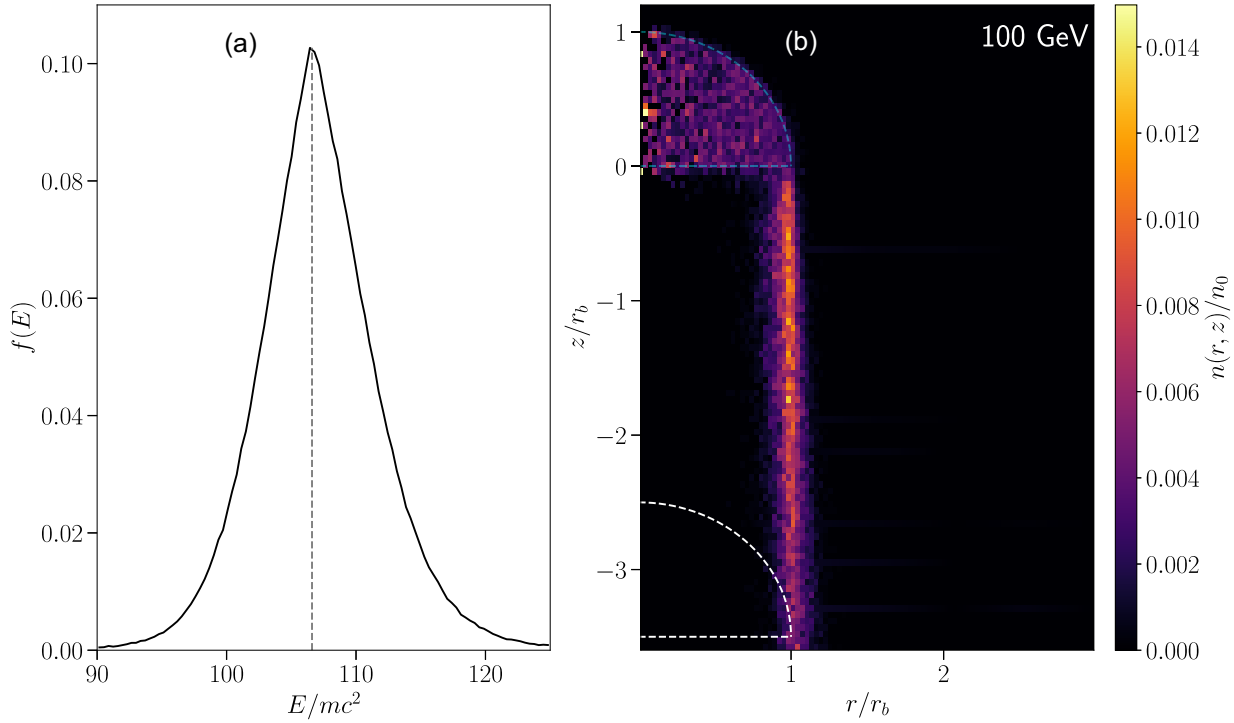

Figure B1. (a) Numerically obtained distribution function, $f(E)$, of CRs (solid line) achieved after the bubble has risen $3.5r_b$. The CRs were initialized at 100 GeV (dashed line). (b) Density $n_{10\ per\ cent}$ of CRs (as in Fig. 2) filtered to highlight only those CRs that have increased their energy by more than 10 per cent.

APPENDIX C: ASYMPTOTIC SOLUTION OF BLASIUS PROBLEM ABOVE BUBBLE

In this appendix, we solve the Blasius problem in the limit

$$\epsilon \equiv \frac{\kappa}{u_b r_b} \ll 1. \tag{C1}$$

The Blasius problem has previously been treated by Churazov & Inogamov (2004) and Xiang et al. (2007) in determining the width of cold fronts due to thermal conduction in a potential flow past a sphere. They solve, analytically, for the steady state of the advection–diffusion equation near the leading edge of the cold front. Their solution confirms that the width of the layer produced in front of the bubble is of the order $\sqrt{\varepsilon} r_b$. Here, we are principally interested in the scaling of the width of the layer at the side of the bubble, since it is this layer that determines the rate of particle loss from the bubble. To determine this width, we show that a solution with a layer of width $\sqrt{\varepsilon} r_b$ exists for all polar angles $\theta \leq \pi/2$, extending the solution of Xiang et al. (2007) away from the top ($\theta = 0$) of the bubble.

In spherical geometry and with the flow specified by equations (A1) and (A2), the steady-state advection–diffusion equation (8) above the bubble ($\theta \leq \pi/2$) becomes

$$-u_b\left(1-\frac{r_b^3}{r^3}\right)\cos\theta\frac{\partial n}{\partial r}+u_b\left(1+\frac{r_b^3}{2r^3}\right)\sin\theta\frac{1}{r}\frac{\partial n}{\partial\theta}$$
$$-\frac{\kappa}{r^2}\left(\frac{\partial}{\partial r}r^2\frac{\partial n}{\partial r}+\frac{1}{\sin\theta}\frac{\partial}{\partial\theta}\sin\theta\frac{\partial n}{\partial\theta}\right)=0. \tag{C2}$$

To show that this equation admits a solution with a layer of thickness $\sqrt{\varepsilon} r_b$, we make the change of variables $r = r_b(1+\sqrt{\varepsilon}x)$ and retain only the lowest-order terms:

$$-3x\cos\theta\frac{\partial n}{\partial x}+\frac{3}{2}\sin\theta\frac{\partial n}{\partial\theta}-\frac{\partial^2 n}{\partial x^2}=0. \tag{C3}$$

Note that, at this order, we have thrown away the polar-diffusion term – the 4th term in equation (C2), which can break the ordering at small θ. This is fine, however, provided we assume $\theta \gg \sqrt{\varepsilon}$ and find a solution that satisfies

$$\left.\frac{\partial n}{\partial\theta}\right|_{\theta\to 0}=0. \tag{C4}$$

We now seek a solution to equation (C3) in the form

$$n(x,\theta)=n_0\left\{1-\mathrm{erf}\left[g(\theta)x\right]\right\}. \tag{C5}$$

This is indeed a *bona fide* solution provided $g(\theta)$ satisfies the differential equation

$$\sin\theta\frac{\partial g}{\partial\theta}=2\cos\theta g(\theta)-\frac{4}{3}g^3(\theta). \tag{C6}$$

To enforce equation (C4) without breaking the ordering of $\partial n/\partial x = \mathrm{O}(1)$, we must therefore have

$$g(\theta\to 0)=\sqrt{\frac{3}{2}}. \tag{C7}$$

Thus, the lowest-order solution above the bubble is given by

$$n(r,\theta,\gamma)=n_0\left\{1-\mathrm{erf}\left[\sqrt{\frac{u_b r_b}{\kappa}}g(\theta)\frac{r-r_b}{r_b}\right]\right\}. \tag{C8}$$

Since $g(\theta)$ is finite between $0 \leq \theta \leq \pi/2$, this ensures that the ordering equation (9) is valid everywhere above the bubble. The numerically integrated solution of equation (C6) for $g(\theta)$ is shown in Fig. C1(a). In Fig. C1(b), the mean radial distance of CRs from the bubble

$$\langle r\rangle(\theta)=\frac{\int_{r_b}^{\infty}r^3 n(r,\theta)\mathrm{d}r}{\int_{r_b}^{\infty}r^2 n(r,\theta)\mathrm{d}r}=r_b+r_b\frac{\sqrt{\pi}}{4g(\theta)}\sqrt{\frac{\kappa}{u_b r_b}}, \tag{C9}$$

is compared, favourably, to the result of our mock simulation above the bubble.

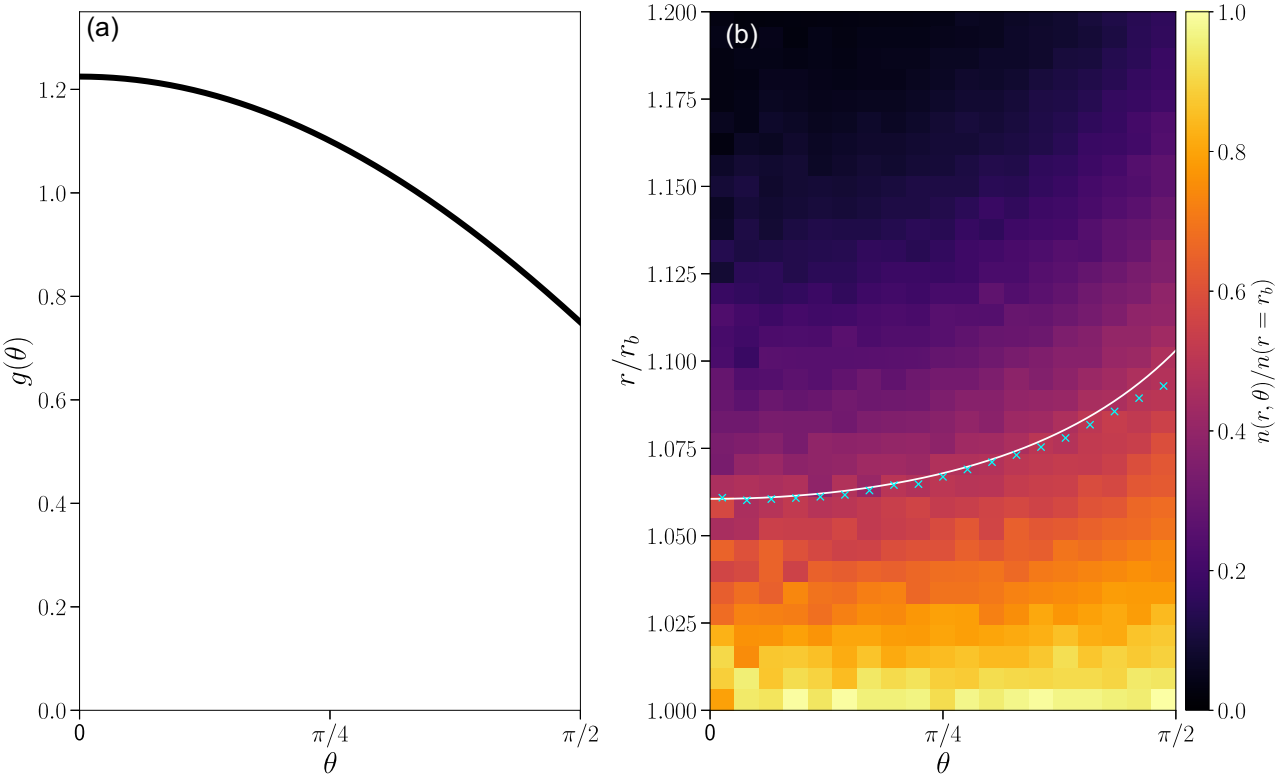

Figure C1. (a) Numerical solution of equation (C6), giving the function $g(\theta)$ that controls the width of the boundary layer around the top of the bubble. (b) Numerical simulation of the density of CRs at 300 GeV outside the bubble assuming volume-filling micromirrors. Crosses show the mean radial distance of CRs from the nominal bubble boundary in each angular interval, and the solid line shows the mean radial distance of CRs from the bubble equation (C9) calculated from equation (C8) with $g(\theta)$ taken from panel (a).

This paper has been typeset from a TEX/LATEX file prepared by the author.